ELSEVIER

Residual stresses, strength and toughness of laminates with different layer thickness ratios

R. Bermejo [a], Y. Torres [a], A.J. Sánchez-Herencia [b], C. Baudín [b], M. Anglada [a], L. Llanes [a,*]

[a] *Departamento de Ciencia de los Materiales e Ingeniería Metalúrgica, ETSEIB, Universidad Politécnica de Cataluña,*
Avda. Diagonal 647, E-08028 Barcelona, Spain
[b] *Instituto de Cerámica y Vidrio (CSIC), C/Kelsen 5, 28049 Madrid, Spain*

Abstract

The effect of residual stresses on the strength, toughness and work of fracture of Al_2O_3–5 wt.% $tZrO_2$/Al_2O_3–30 wt.% $mZrO_2$ layered ceramics with different thickness ratios has been investigated. The laminates, as well as a monolithic Al_2O_3–5 wt.% $tZrO_2$ used as reference material, were fabricated by sequential slip casting. Residual stresses were estimated experimentally using indentation techniques and analytically using a three-dimensional finite element model. Flexural strength was evaluated by means of four-point bending tests on specimens with natural and artificial (indentation) flaws. Experimental findings show the existence of a threshold strength in the laminates whose value depends on the layer thickness ratio. Crack growth resistance behaviour was studied by crack opening displacement-controlled tests and by recourse to a weight function analytical approach. The high compressive stresses in the internal layers yield a pronounced R-curve behaviour in the laminates. Regarding work of fracture, it is found to be enhanced to levels up to about six times that of the reference monolith. The results are discussed in terms of the optimum layered architectural design for structural applications on the basis of the compromise between threshold strength and energy absorption capability associated with crack bifurcation mechanisms occurring at fracture.
© 2006 Acta Materialia Inc. Published by Elsevier Ltd. All rights reserved.

Keywords: Multilayers; Residual stresses; Fracture; Threshold strength; Toughness

1. Introduction

Design against brittle-like fracture assumes that materials contain defects either within the bulk or at the surface, resulting from processing and/or machining procedures. This is specifically true for ceramic components where intrinsic or extrinsic flaws are the common source of failure due to the stress concentration associated with them. From this perspective, it is well established that the stress concentration at a crack tip depends on crack geometry; hence, the size and type of these defects will condition the mechanical strength of the material. As a result, structural ceramics exhibit a statistically variable brittle fracture which

limits their use for load-bearing applications. In the last three decades, remarkable advances have been achieved to overcome the lack of toughness of structural ceramics. Several processing routes have emerged which do not recall conventional "flaw elimination" approaches, but rather "flaw tolerant" ones based on the operability of energy release mechanisms aiming to improve strength reliability. Among those, doping, fibre and/or particle reinforcement, functional grading and layered architectural design may be highlighted. Particularly, alumina–zirconia [1,2] and mullite–alumina [3] ceramic composites with a layered structure, among others, have been reported to exhibit increased apparent fracture toughness and energy absorption, as well as non-catastrophic failure behaviour.

One of the most used multilayer designs that ensures higher apparent toughness is that which combines layers

---

* Corresponding author. Tel.: +34 93 4011083; fax: +34 93 4016706.
E-mail address: luis.miguel.llanes@upc.edu (L. Llanes).

with different volume changes during cooling from the sintering temperature. Under these conditions, an alternate tensile–compressive residual stress state develops with specific location of the compressive layers, either at the surface or internally, depending on the attempted design approach, based on either mechanical resistance or damage tolerance, respectively. In the former case, the effect of the compressive residual stresses on the nominally applied stress results in a higher, but single-value, apparent fracture toughness together with enhanced strength (the main goal) and some improved reliability [4,5]. On the other hand, in the latter case, the internal compressive layer is microstructurally designed to rather act as stopper of any potential processing flaw at surface layers, independent of original size and location, such that failure tends to take place under conditions of maximum crack growth resistance. As a consequence, strength becomes flawsize independent and reliability is significantly increased. Within this framework, an "extreme" case is the possibility of developing materials exhibiting a "threshold strength", i.e. a stress below which failure would not occur despite the presence of relatively large cracks, as reported for alumina–alumina mullite [6,7] or alumina–alumina zirconia multilayered systems [8]. From this viewpoint, much effort has been expended on the fabrication of laminates with a tailored residual stress profile arising from mismatch of thermal expansion coefficients between layers, selective phase transformation and/or chemical reactions [7,9,10]. In these investigations, zirconia-containing laminar ceramics have been employed to develop compressive stresses in the internal layers by means of the tetragonal to monoclinic phase transformation that takes place in the zirconia phase when cooling down during sintering. The corresponding volume increase associated with such transformation determines the residual stress field within the multilayer. Under certain conditions, these compressive stresses may act as a barrier to crack propagation. In other cases, crack deflection at the interface of dissimilar materials [11–13] and/or crack bifurcation due to the high compressive stresses in the internal layers of the composite [14,15] result in an increase of fracture toughness and energy absorption capability [16]. The search of laminar ceramic composites for structural applications must be focused on "flaw tolerance" materials, where reliability gets significantly enhanced, exhibiting a fairly high resistance to failure.

The purpose of the investigation reported here was to optimize the design of alumina–zirconia layered ceramics to obtain flaw-tolerant materials with pronounced crack growth resistance and work of fracture. In doing so, three multilayered architectures of the same composition but different layer thickness ratios fabricated by slip casting were studied. The residual stress profile was determined both experimental and analytically using the indentation technique and a three-dimensional finite element model, respectively. Four-point bending tests were performed on virgin and indented samples to account for the existence of a threshold strength in the laminates. Although no standardized methods are available to evaluate the fracture toughness in layered composites, a fracture mechanics weight function analysis was effectively used to estimate the crack growth resistance behaviour (R-curve) as a function of position within the layered architectures investigated. Additionally, crack opening displacement (COD)-controlled tests were conducted to determine the work of fracture in monoliths and laminates. Finally, a discussion of the optimum multilayered architectural design is provided in terms of threshold strength, toughness and energy absorption capability associated with energy-dissipating mechanisms operative during initial crack extension up to final catastrophic failure.

2. Experimental

2.1. Materials

The following starting powders were used: (i) α-alumina (Condea, HPA05, USA) with 0.29 μm average particle size and 8.5 m^2/g specific surface area (N_2 adsorption; BET method), (ii) Y_2O_3-free and Y_2O_3 (3 wt.%)-stabilized zirconia (TZ-0 and TZ-3YS, Tosoh, Japan) with 0.60 and 0.37 μm average particle size and 14.0 and 6.7 m^2/g specific surface area, respectively. A slurry composed of Al_2O_3/5 vol.% Y_2O_3-stabilized ZrO_2 (t-ZrO_2), referred to as ATZ, was used to form all the thicker layers. The t-ZrO_2 was utilized to control the grain size of the Al_2O_3 during sintering. In order to form the thin layers a slurry containing Al_2O_3/30 vol.% Y_2O_3-free ZrO_2 (m-ZrO_2), named AMZ, was employed. Each suspension was re-used every time to form the successive layers of the corresponding composition. The content of non-stabilized zirconia in these layers was selected to promote high residual compressive stresses, as studied in previous works [15,17,18]. Preparation of the batches has already been detailed elsewhere [19]. Wall thickness vs. time curves were experimentally determined on monolithic samples for both slurries and then used to calculate the time for sequential slip casting of three different multilayered systems named A, B and C, with the same composition but different layer thickness ratios [20]. Laminates were composed in all cases of five thick ATZ layers alternated with four thin AMZ layers. Cast specimens were carefully removed from the moulds, dried at room temperature for 48 h, and finally fired at 1550 °C for 2 h using heating and cooling rates of 5 °C/min. Rectangular plates of approximately 60 mm × 60 mm × 4 mm were obtained for the three multilayered architectures. The thickness of the layers resulting for each case was measured by optical microscopy on polished samples, and the experimental values, including the corresponding layer thickness ratios, are listed in Table 1. The outer ATZ layers were cast thicker than the inner ones to allow grinding and polishing procedures. Density measurements were carried out for both ATZ monoliths and laminates, yielding values of 99.5% and 99.3%, respectively.

Table 1
Layer thickness and thickness ratio of the multilayered systems A, B and C

Multilayer	Layer thickness (μm)		Thickness ratio (ATZ:AMZ)
	ATZ	AMZ	
A	650 ± 10	140 ± 5	4.6
B	540 ± 10	95 ± 5	5.7
C	570 ± 10	60 ± 5	9.5

2.2. Residual stress determination

In every case where dissimilar materials are sealed together and subsequently undergo differential dimensional change, stresses arise between them [21]. For a multilayered system composed of n layers of composition X and thickness t_x and $n-1$ layers of composition Y and thickness t_y, the residual stress values in the bulk of each layer may be estimated as [22]

$$\sigma_x = \Delta\varepsilon \frac{E'_x}{1 + \frac{E'_x n t_x}{E'_y (n-1) t_y}} \tag{1}$$

$$\sigma_y = -\Delta\varepsilon \frac{E'_y}{1 + \frac{E'_y (n-1) t_y}{E'_x n t_x}} \tag{2}$$

where $E'_i = E_i/(1 - v_i)$, E_i being Young's modulus and v_i Poisson's ratio of a given layer. As evidenced from the above equation, the magnitude of the residual stresses generated in these systems depends on both the relative thickness of the layers (t_x/t_y) and the difference in thermal strain between adjacent layers, $\Delta\varepsilon$. As mentioned before, this residual thermal strain may be due to mismatch of thermal expansion coefficients between layers, selective phase transformations and/or chemical reactions. In this investigation, non-stabilized zirconia has been utilized in the thin AMZ layers to generate a significant thermal mismatch between layers due to the $t \rightarrow m$ zirconia phase transformation occurring when cooling down during sintering. This martensitic transformation is accompanied by an increase in volume which modifies the cooling shrinkage behaviour of the laminate, developing compressive stresses inside the thin layers and tensile stresses in the thicker ones.

In order to evaluate experimentally the residual stress profile in the multilayers investigated, the indentation technique was employed. Several Vickers indentations with a load of 30 N were applied in the three laminates at different distances from the ATZ/AMZ interface. The cracks normal to the ATZ/AMZ interface, emanating from such indentations, were measured using interference contrast. To determine the crack tip position for each indentation crack, the light beam was reduced so that the crack tip was in the dark field next to the beam area. The magnitude of the residual stresses in the inner and outer ATZ layers of each laminate was determined by equating the critical stress intensity factor, K_{Ic}, for indentation cracks on a stress-free ceramic [23] and on a ceramic within a residual stress field [24]. Thus, The following equation is obtained

and used to calculate the residual stresses, σ_{res}, through the layers of the laminates:

$$\sigma_{res} = \frac{1}{\psi\sqrt{c}} K_{Ic} \left[1 - \left(\frac{c_o}{c} \right)^{3/2} \right] \tag{3}$$

where c_o and c are the indentation crack lengths in the ATZ monolith and in the ATZ layers of the laminate, respectively, ψ is a crack-shape factor that can be calculated for a given geometry (in this case $\psi = 0.90$, as determined for a similar multilayer composite on a previous study [25]), and K_{Ic} is the fracture toughness obtained by the indentation method in the corresponding ATZ monolithic material [8].

Additionally, a finite element analysis previously developed [26] was implemented in order to determine the residual stress profile within the tri-dimensional multilayered structures. In doing so, prismatic bar-shaped specimens were modelled as representative of the samples utilized in the experiments for material characterization. The sintering step was simulated attempting to quantify the thermal strain mismatch during cooling and the corresponding residual stress field in the layered materials under investigation. The finite element model employed was a nine-layer structure, whose layer properties, i.e. Young's modulus and thermal expansion coefficient, were taken as those of the monolithic ATZ and AMZ samples. All materials were assumed to be isotropic so that only two independent mechanical properties, Young's modulus and Poisson's ratio, had to be provided. Young's moduli for the ATZ and AMZ layers were taken as those experimentally determined by the impulse excitation technique on the corresponding monoliths [25], i.e. 390 and 280 GPa, respectively. A Poisson's ratio of 0.22 was used for all the layers. Regarding thermal properties, the thermal expansion coefficients ($\alpha_{ATZ} = 9.82 \times 10^{-6} \text{ K}^{-1}$ and $\alpha_{AMZ} = 8.02 \times 10^{-6} \text{ K}^{-1}$) were discretely introduced in the model from data corresponding to dilatometry curves, considering 1250 °C as the reference stress-free state, i.e. the temperature above which residual stresses are negligible [25]. The residual stress profile was computed both at the centre of the laminates and at the surface, in order to account for the edge stress effects in the composites [27].

2.3. Flexural strength tests

The modulus of rupture (MOR) of the three laminates was evaluated under four-point bending tests performed on prismatic bars and compared to that of the ATZ monolith, taken as reference. Five specimens of each kind were used for strength determination. In doing so, a fully articulated test jig with inner and outer spans of 10 and 20 mm, respectively, was used. Tests were carried out under load control using a servohydraulic testing machine (model 1341, Instron Ltd.) with a load cell of 20 kN at a rate of 100 N/s. All the fractured specimens were inspected using both reflected light optical microscopy and scanning electron microscopy (JEOL JMS 6400) to determine the type,

size and location of the failure-controlling natural flaws. The mechanical strength for the three laminates, σ_f^A, σ_f^B and σ_f^C, and the reference monolith, σ_f^{ATZ}, is based on the evaluation of the failure stress at the location of the discerned critical natural flaw. The stress distribution under four-point bending on a prismatic bar formed by layers with different elastic properties was taken into account following the expression given by [28]

$$\sigma_{i,y} = \frac{E_i M}{(EI)}(y - y_{na}) \tag{4}$$

where E_i is Young's modulus of the corresponding layer, M is the moment for the case of four-point bending tests ($M = Fl$, where F is the applied load and l the distance between inner and outer spans), y_{na} is the position of the neutral axis on a multilayer, y is the specimen depth where the failure stress is to be determined (at the location of the critical flaw) and EI is the flexural rigidity of the layered composite calculated for bending perpendicular to the layer plane.

In order to evaluate the threshold strength and R-curve behaviour in the laminates investigated, four specimens from each multilayered system were ground and polished up to 3 μm both at the surface and at one of their lateral faces. Four different combinations of Vickers indentations were placed longitudinally on each specimen surface with an offset separation distance of 2 mm to avoid any crack interaction: (a) 200, 200, 100, 50 N; (b) 150, 150, 100, 50 N; (c) 100, 100, 50, 30 N; and (d) 50, 50, 30, 30 N. The same procedure was conducted on ATZ monoliths for comparative purposes. The indentation crack length was measured using an optical microscope by recourse to Nomarski interference contrast. Finally, all the specimens were fractured under four-point bending. The failure stress for the indented specimens (σ_{Ri}) was calculated using Eq. (4), which for the case of the laminates takes into account the different elastic properties of the corresponding layers. In all cases, a post-mortem examination was made to confirm failure initiation from the indentation sites and not from either interface defects or other surface flaws.

2.4. Tests under COD control

The work of fracture of the laminates and the reference ATZ monolith was determined by testing notched samples in three-point bending under COD control, at a rate of 1 μm/s. Identical specimens for monoliths and laminates were notched using a razor blade automatic machine. Notches were machined to enter a small depth, 150 μm, into the ATZ phase, and a COD-gauge was attached to the specimen surface at the notch site to register the COD data. Additionally, the extension of the crack in the single-edge-V-notch-bend (SEVNB) specimens was continuously monitored using a long-distance focal optical microscope (Questar QM100) with an effective magnification of ×1000, and the data recorded by software (Labview 6.1) coupled to the testing set-up.

3. Results and discussion

3.1. Residual stress profile

The variation of the experimentally measured indentation crack length for the three laminates, as a function of the distance to the interlayer, is presented in Fig. 1. The magnitude and distribution of the residual stresses within the inner and outer ATZ layers of the laminates, determined using Eq. (3), are shown in Fig. 2. For the internal ATZ layers a symmetrical parabolic distribution is obtained, reaching a maximum value close to the ATZ/AMZ interfaces. On the other hand, for the outer layers, residual stresses decrease when the free surface is approached. Experimental limitations due to the small dimensions of the AMZ layers hindered the study of the empiric residual stress profile in these thin compressive layers.

It is well known that stresses at the free surface of layered materials are different from those within the bulk. While the stresses determined by the indentation method are valid for the surface of the specimens, the stress profile calculated with the three-dimensional finite element model describes the residual stress distribution through the layers both in the bulk and at the surface of the three laminates
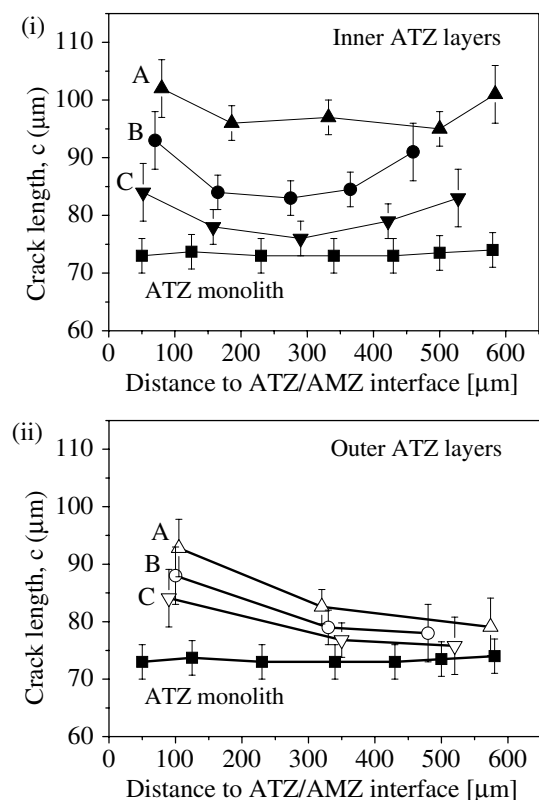

Fig. 1. Experimentally measured values of the indentation crack length, as a function of the distance to ATZ/AMZ interface, in: (i) inner ATZ layers of the systems A (▲), B (●), C (▼) and ATZ monolith (■); and (ii) outer ATZ layers for the three systems A (△), B (○), C (▽) and for the ATZ monolith (■).
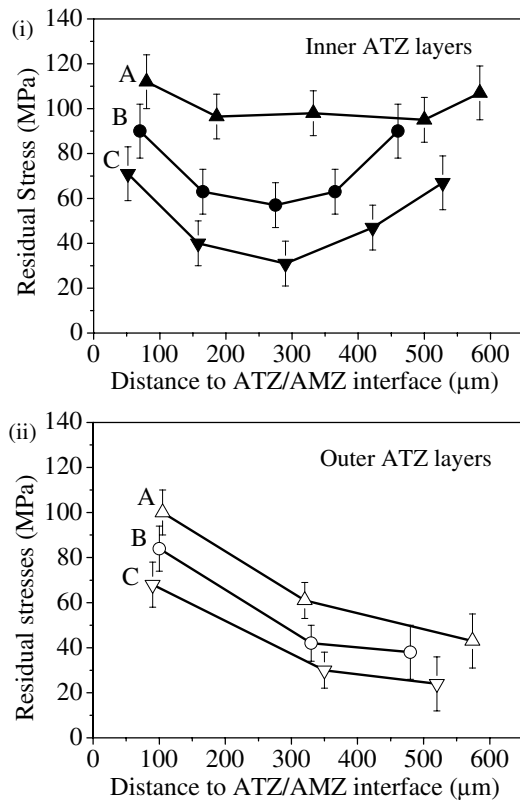
Fig. 2. Plot of the experimentally measured residual stress profile in: (i) inner ATZ layers of the multilayers A (▲), B (●), C (▼); and (ii) outer ATZ layers of the three systems A (△), B (○), C (▽).

(Fig. 3). From the referred plots it can be inferred that the residual stress profile at the surface is similar to that determined experimentally with indentations. On the other hand, stresses in the bulk show the same distribution within each layer, ranging from 60 to 120 MPa in the tensile layers and from −720 to −680 MPa in the compressive ones, depending on the laminate studied. These values are in good agreement with those calculated using Eqs. (1) and (2), as listed in Table 2. As expected, increasing thickness ratio results in a strong decrease of the tensile stresses in the ATZ layers together with a slightly rise of the compressive stresses in the AMZ ones. From a residual stress viewpoint, multilayer type C would be the best candidate for structural applications, among the ones studied here, since it combines the highest compressive stresses in the internal layers with the lowest tensile ones at the surface.

3.2. Fracture behaviour

3.2.1. Strength and fractography

Fractographic observations of the fractured specimens showed differences in the natural flaw populations for ATZ monoliths and laminates. Fig. 4 shows the fracture surfaces and the natural defects of some representative specimens tested under four-point bending. Even though pores were the critical defects in both series of materials, those present in the monoliths were smaller, with maximum
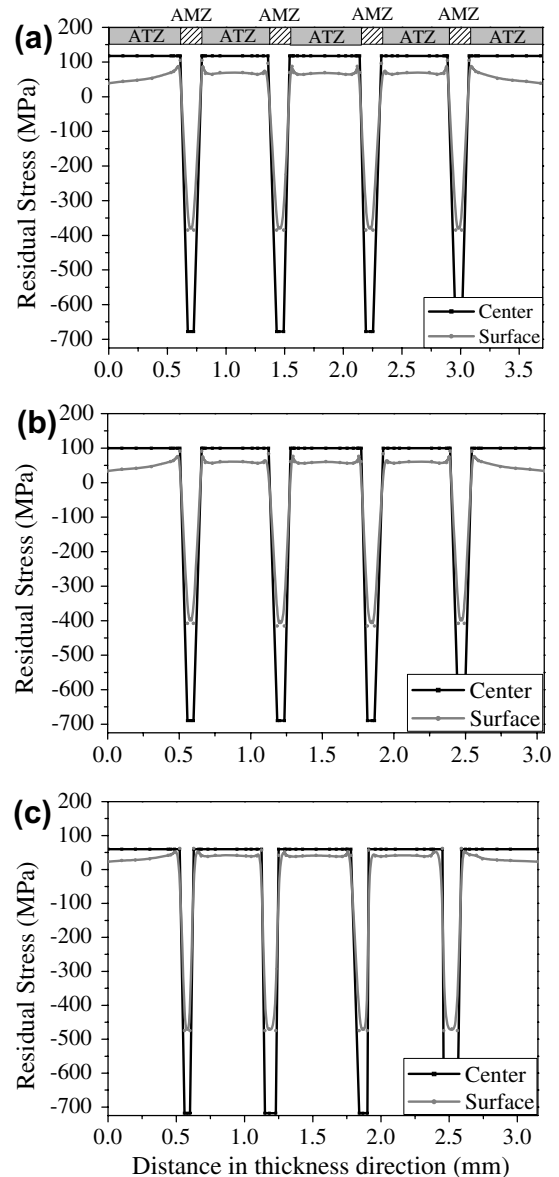

Fig. 3. Stress distribution through the layers in the bulk and at the surface of the multilayers (a) A, (b) B, and (c) C, calculated using a three-dimensional finite element model.

Table 2
Analytical residual stresses calculated in the bulk material for the A, B and C multilayered systems

Multilayer	Tensile residual stress (MPa)	Compressive residual stress (MPa)
A	116	−678
B	97	−691
C	60	−718

diameters ranging from 30 to 75 μm, less irregular, and located closer to the surfaces (Fig. 4a). On the other hand, pores in the laminates (Fig. 4b–d) were much larger, with maximum diameters ranging from 90 to 185 μm, and more irregular, such as those formed by differential sintering in compacts with large agglomerates. It is clear that removal
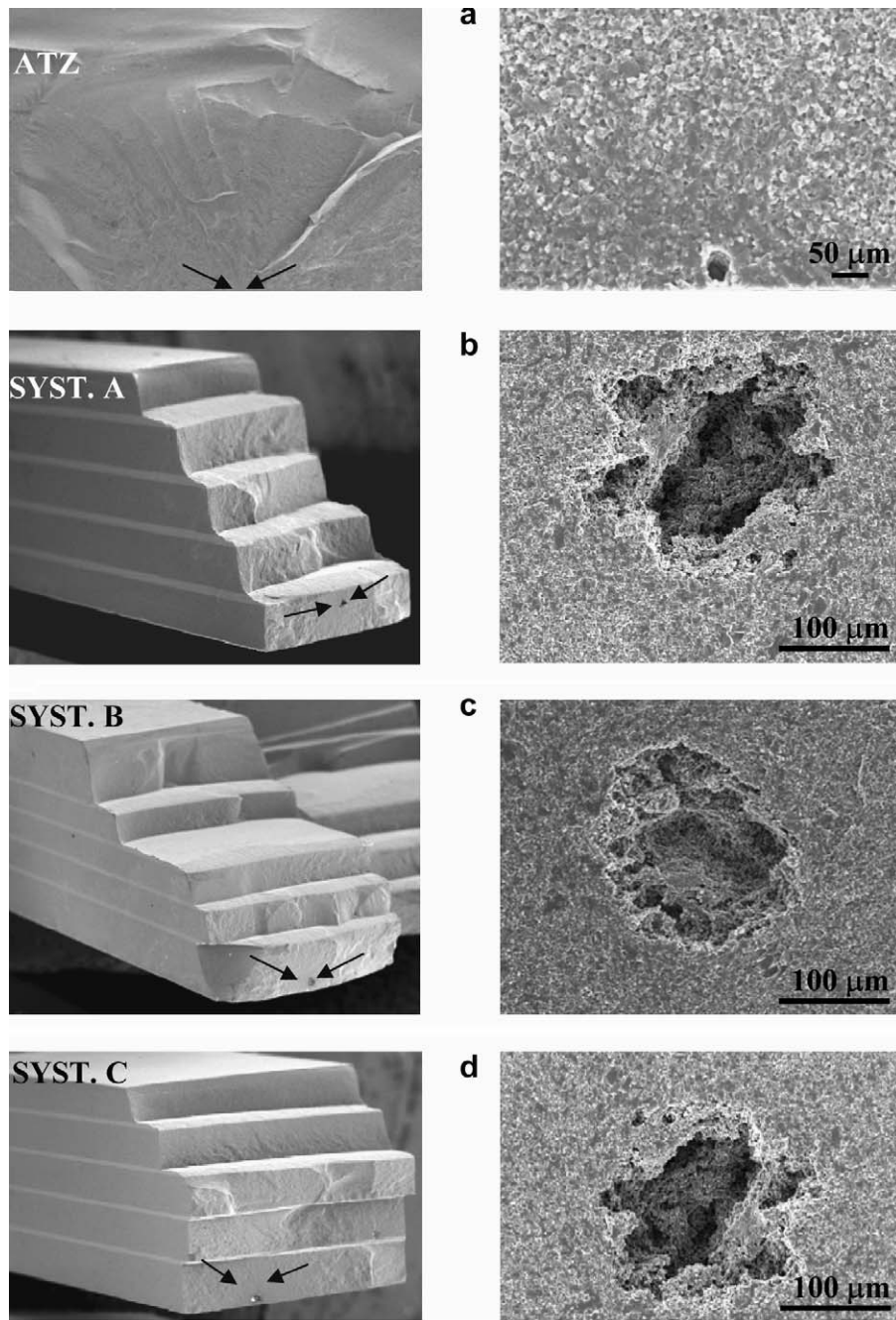
Fig. 4. Scanning electron micrographs of fracture sites for the ATZ monolith and laminates A, B and C. Natural flaws in the laminates (b–d) are located at different locations within the outer most ATZ layer and are larger than those in the ATZ monolith (a). The propagation of the critical flaws in systems A and B is more stepped than in system C, whereas it may be described as flat for the case of the ATZ monolith.

of these agglomerates, formed during the sequential casting step, should be a key action for optimizing the processing procedure of the laminates investigated here.

Following the above ideas, a description of the fracture behaviour of ATZ monoliths and laminates was attempted in terms of unstable propagation of natural flaws within a linear elastic fracture mechanics (LEFM) framework. Such an approach was implemented by considering monoliths and laminates as brittle materials and their fracture occurring from pre-existing natural flaws of critical size $2a_c$, according to the generic relationship

$$K_{Ic} = Y\sigma_f\sqrt{\pi a_c} \tag{5}$$

where K_{Ic} is the plane strain fracture toughness, σ_f is the fracture resistance and Y represents a geometrical factor that depends on the configuration of the flawed sample and the manner in which the loads are applied. Although in applying LEFM criteria it is common to assume fracture-controlling flaws as if they were circular cracks, it is clear from Fig. 4 that failure origins for the materials studied here are pores, i.e. defects with aspect quite different from such simple geometry. Within this context, one

interesting approach is the consideration of the whole flaw (with an effective crack extension of $2a$) as an spherical defect (pore of diameter $2R$) acting as a stress concentrator on a circumferential "small" crack (of length b) around it [29,30]. Various studies are available on the stress intensity factor for such a configuration [29,31,32]. For simplicity, the relation between the "normalized stress intensity factor" (K/σ) and the "normalized crack length" (b/R), as given in Fig. 4 of Ref. [29], is here fitted to the following equation:

$$g(b/R) = \frac{2.51 + 2.34(b/R)}{1 + 3.87(b/R)} \qquad (6)$$

and directly implemented within a relationship as the one given in Eq. (5), but under the consideration of critical flaw size in terms of the length of the circumferential crack at failure (b_c):

$$K_{Ic} = g(b/R)\sigma_f \sqrt{\pi b_c} \qquad (7)$$

Indeed, this is an important variable in the model because, upon load application, it sets the value of the applied stress intensity factor around each pore. As it has been previously stated for other polycrystalline ceramics [33–36], a correct approximation of the size of this crack requires an exhaustive evaluation of the microstructure at the fracture origin. For the particular case of the ATZ investigated, with Al_2O_3 and ZrO_2 grain sizes of 2.0–3.0 and 0.3–0.6 μm, respectively, its intrinsic fine microstructure makes it difficult to clearly determine the extension, and even the existence, of such cracks. However, they may be speculated to exist once thermal expansion mismatch between neighbouring grains and phase transformation of zirconia particles, upon cooling from processing, are accounted for. In this work the appropriate size of the crack length was first estimated from calibration of the fracture mechanics model within the residual stress-free ATZ monolith, and subsequently implemented for analysing the fracture behaviour of the laminates. In doing so, direct experimental data for the ATZ monolith (i.e. flexural strength and critical flaw size, as given in Table 3; and a fracture toughness value of 3.2 MPa m$^{1/2}$, as measured by the SEVNB method in a previous work [8]) were incorporated as inputs within Eq. (7), yielding as a result a best-fitting b value of 5 μm, i.e. a crack

extension of about twice the microstructural scale of the ATZ under consideration.

Concerning the laminates, as a first approach the value of 3.2 MPa m$^{1/2}$ was considered as the intrinsic fracture toughness of the ATZ layers of the three multilayered systems. Under these conditions, the expected applied stress at fracture for each multilayered architecture, σ_{appl}^c, could be estimated using Eq. (7), once the residual stress state inherent to the outer ATZ layers (as reported in Table 2) is taken into account. Thus, fracture of laminates originating at pores might be described as

$$K_c = [g(b/R)](\sigma_{res} + \sigma_{appl}^c)\sqrt{\pi b_c} \qquad (8)$$

where K_c is assumed to be the K_{Ic} for the ATZ material, $g(b/R)$ is given by Eq. (6) under the consideration of the effective critical flaw sizes experimentally discerned at the corresponding fracture surfaces, σ_{res} is the tensile stress in the outer ATZ layer for each layered system and b_c is taken as 5 μm. The critical σ_{appl}^c values extracted from Eq. (8) are listed in Table 3 and would represent the expected failure stress of each multilayered architecture assuming that: (i) propagation of natural flaws becomes unstable within the outer ATZ layer, and thus, controls failure in these layered systems; and (ii) the intrinsic fracture behaviour of this layer is exactly the same as the one exhibited by the bulk ATZ monolith. Table 3 also includes, for comparative purposes, the experimental fracture strength σ_f obtained under four-point bending.

From the data given in Table 3, several aspects may be highlighted. First, the critical σ_{appl}^c values predicted for the laminates, considering their fracture behaviour as governed by the ATZ outer layer mechanical properties, are 4–17% lower than the failure stress σ_f obtained under four-point bending tests. Such a finding suggests that the layered structure itself (below the failure-controlling defect) acts as reinforcement in terms of strength, with respect to the ATZ monolithic material, despite the tensile residual stresses induced within the outer ATZ layer. Second, although the experimental failure stress for the ATZ monolith is higher than for the multilayered materials, as associated with the different critical defect size above discussed, the corresponding strength scatter decreases in the latter, from 13–14% to about 3–5%. Indeed, this is sound evidence of the beneficial effect induced by the layered architectural design from a damage tolerance perspective (as discussed below). The strength values measured on the laminates represent a clear indication of a reliable failure stress, as reported for other multilayered structures designed with internal compressive stresses where the strength variability described by the Weibull modulus underlined the high reliability of the layered materials [7]. Within this context, a very interesting observation came from the fact that the examined fracture surfaces of the laminates showed initial crack growth of the natural flaws up to the first AMZ layer, before catastrophic failure, as seen in Fig. 5. Hence, the true critical flaw size a_c (at fracture) became as deep as

Table 3
Effective failure strength parameters for the laminates and the monolithic ATZ

Material	σ_f (MPa)	σ_{res} (MPa)	σ_{appl}^c (MPa)	$2a_c$ (μm)
ATZ	482 ± 65	0	487 ± 47	58 ± 15
Laminate A	326 ± 15	116	271 ± 21	145 ± 40
Laminate B	360 ± 14	97	299 ± 22	128 ± 35
Laminate C	343 ± 12	60	329 ± 16	142 ± 32

Experimentally measured flexural strength σ_f; residual stress σ_{res} within each ATZ layer; expected critical applied stress σ_{appl}^c considering the failure-related external ATZ layers in the laminates as ATZ monoliths; and range of critical natural flaw sizes $2a_c$ as discerned from scanning electron microscopy fractographic examination.

the thickness of the outer ATZ layer of the corresponding multilayered system, i.e. the initial flaw is able to experience an initial extension up to the ATZ/AMZ interface, with Y changing as the crack dimensions increase. The effective geometrical factor Y ascribed to such critical flaw was evaluated from the empirical equations proposed by Newman and Raju [37] for a semielliptical surface crack of depth a and width $2c$, by using a crack geometry aspect ratio (a/c) of about 1, as determined from experimentally measured values in the fracture specimens. Within this framework, the LEFM approach was also implemented through Eq. (5) to estimate the stress intensity factor K_c evaluated at the ATZ/AMZ interface of each laminate, using the failure stress value calculated at the flaw site given by Eq. (4). The results are shown in Table 4. Although there were no clear differences in K_c among the three layered systems, there exists a significant increase in the apparent fracture toughness of the laminates with respect to that evaluated for the ATZ monolith. This increase in toughness must be related to the presence of the thin AMZ compressive layers, which act as a well-defined barrier to flaw propagation through the material. It leads to a "single-value" critical flaw size at failure, and consequently would suggest the presence of a threshold strength in the laminates investigated. Moreover, observation of the fracture surfaces revealed a different pattern on the crack propagation when comparing the ATZ monolith and the laminates. In the former, similar to the finding expected in conventional brittle materials, a
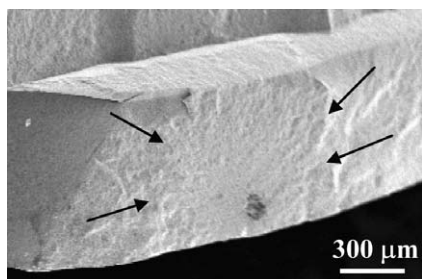

Fig. 5. Detail of the initial growth of a natural flaw up to the first AMZ layer for a multilayer type B, before catastrophic failure.

Table 4
Fracture mechanics data and work of fracture for the laminates and monolithic ATZ

Material	σ_f (MPa) at flaw site	a_c (μm)	K_c (MPa m$^{1/2}$)	γ_{WOF} (J/m^2)
ATZ	482 ± 65	29 ± 15	3.2 ± 0.2	22
Laminate A	240 ± 15	650 ± 10	7.3 ± 0.3	77
Laminate B	250 ± 14	540 ± 10	7.5 ± 0.2	126
Laminate C	254 ± 12	570 ± 10	7.3 ± 0.2	102

Critical stress intensity factor values, K_c, are calculated by recourse to Eq. (5), considering the outer ATZ layer thickness as the critical flaw size a_c, for the laminates; or by implementing Eq. (7), as related to an intrinsic defect of effective flaw size $2a_c$, for the monolithic ATZ. In all the cases, failure stress at the flaw site was determined through Eq. (4). Finally, work of fracture, γ_{WOF}, was estimated from the integration of the registered load–displacement curve per unit volume for the ATZ monolith as well as for the three laminates.

straight fracture surface was discerned (Fig. 4). On the other hand, the three laminates showed a step-like fracture, being more pronounced in systems A and B than in system C (as seen in Fig. 4). The main reason for such observation may be found in the evidence of deflection and/or bifurcation when the corresponding propagating crack interacts with the thin AMZ layers under compression, as seen in Fig. 6 for laminate type B. The bright regions in the top-view of Fig. 6 shows the extent of such crack bifurcation along the AMZ layers. This phenomenon might increase the fracture energy and thus the toughness of the material, as demonstrated by other authors for other multilayered systems [12,16]. From this viewpoint, it should be emphasized that bifurcation was observed at fracture for all the laminated materials studied. Such a finding was expected for multilayers type A and B, since edge cracking had been previously developed in these two systems along the centre of the AMZ compressive layers [6,14,17]. On the other hand, although system C did not show a very pronounced step-like fracture surface (see Fig. 4), crack bifurcation was also encountered even for specimens where edge cracking had not been previously detected. This is an important finding since these two mechanisms have been always been thought to be related [38,39]. Following the above considerations, the mechanical characterization study was further extended in the layered architectures to evaluate the existence of a threshold strength and the corresponding crack growth resistance (R-curve) behaviour.

3.2.2. Threshold strength and R-curve behaviour

Indentation strength tests were carried out to evaluate the presence of a threshold strength in the laminates, as suggested by the above discussion due to the crack arrest experienced by the natural flaws at the first ATZ layer, i.e. existence of a "single-value" flaw size associated with the failure of the specimens. Fig. 7 represents the variation of the failure stress with the indentation load applied for the ATZ monoliths and for the three laminates studied. A linear regression analysis was implemented to obtain the best fit for the experimental data. As it can be inferred from the plot, the failure stress values, σ_f, decrease in the
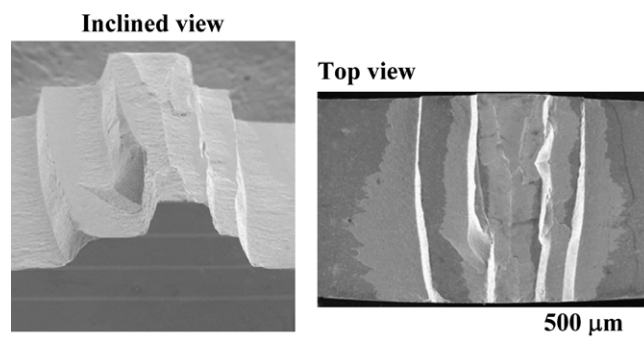

Fig. 6. Views of a multilayered type B fracture site. Step-like fracture is observed due to the bifurcation of the propagating crack when entering the AMZ layers (bright contour at the top view).
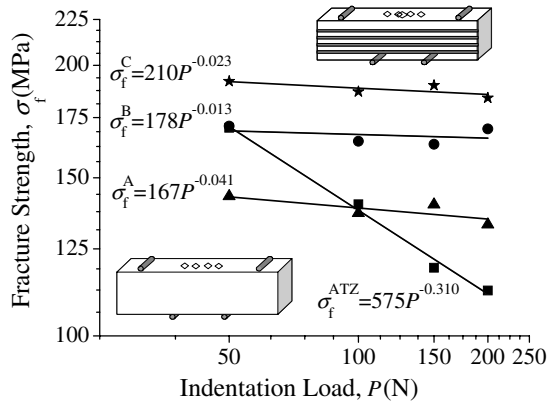
Fig. 7. Plot of the variation of the failure stress under four-point bending σ_{f}, with the indentation load, P, for indented ATZ monoliths (■) and the multilayered systems A (▲), B (●) and C (★).

ATZ monoliths with the indentation load applied, P, following a power law, $\sigma_{\mathrm{f}} \propto P^{-k}$, with $k = 0.31$. This value is very close to 1/3, which corresponds to the behaviour expected in brittle materials exhibiting a flat R-curve (single-valued toughness) [40]. On the other hand, the exponent k values for the three laminates are much lower than 1/3, suggesting a very steep R-curve behaviour. Moreover, the almost constant value of σ_{f} in the laminates points out the existence of a threshold strength, regardless of the indentation flaw size, reaching its highest value for multilayers type C, i.e. layered architectures with relatively higher compressive stresses. From these findings, it can be concluded that threshold strength is dictated by the magnitude of the compressive stresses present in the thin AMZ layers and, from this perspective, material type C results to be the optimum "flaw tolerance" design in terms of strength.

Although no standardized methods are available to evaluate the fracture toughness in layered composites, a fracture mechanics weight function analysis has been effectively used to estimate the crack growth resistance behaviour (R-curve) as a function of the position of an edge crack within each multilayered system investigated with a residual stress distribution, $\sigma_{\mathrm{res}}(x)$. The so-called apparent fracture toughness (since it is influenced by the residual stresses), $K_{\mathrm{apt,c}}$, may be defined as follows:

$$K_{\mathrm{apt,c}} = K_{\mathrm{Ic}} - \int_0^a h(a,x)\sigma_{\mathrm{res}}(x)\,\mathrm{d}x \qquad (9)$$

where K_{Ic} is the intrinsic fracture toughness of each individual layer calculated by the SEVNB method in the corresponding monoliths (2.6 and 3.2 MPa m$^{1/2}$ for the AMZ and ATZ layers, respectively), x is the distance along the crack length measured from the surface, a is the crack length, and $h(a,x)$ is a weight function, as developed by Fett and Munz [41] for an edge crack in a bar, commonly employed in the evaluation of R-curve behaviour for multilayered systems. The corresponding weight function is given by

$$h(a,x) = \left(\frac{2}{\pi a}\right)^{1/2} \frac{1}{\left(1 - \frac{x}{a}\right)^{1/2}\left(1 - \frac{a}{W}\right)^{3/2}}$$

$$\times \left[\left(1 - \frac{a}{W}\right)^{3/2} + \sum A_{v\mu}\left(1 - \frac{x}{a}\right)^{v+1}\left(\frac{a}{W}\right)^{\mu}\right] \qquad (10)$$

where W is the specimen thickness, and the coefficients $A_{v\mu}$ and exponents v and μ are determined using the "boundary collocation method", as described elsewhere [41]. Integrating this weight function for the geometries under study, the apparent fracture toughness was determined as a function of a crack length parameter $\hat{a}$, defined as $Y\sqrt{a}$, with Y given by [42]

$$Y(\alpha) = \left[\frac{1.99 - \alpha(1-\alpha)(2.15 - 3.93\alpha + 2.7\alpha^2)}{(1+2\alpha)(1-\alpha)^{3/2}}\right]; \quad \alpha = a/W \qquad (11)$$

Fig. 8 represents the $K_{\mathrm{apt,c}}$ curve corresponding to a multilayered B architecture. The trend of the $K_{\mathrm{apt,c}}$ curve is in good agreement with previous analysis on multilayered structures reported in the literature [43–45]. It can be observed that $K_{\mathrm{apt,c}}$ decreases in the layers with a tensile residual stress state and increases rapidly within the layers with compressive residual stresses as $\hat{a}$ increases. In this regard, although microstructure-related mechanisms such as crack bridging may influence the increase in the crack growth resistance in multilayered alumina–zirconia composites (as demonstrated by Moon et al. [44]), the main contribution is due to the macroscopic residual compressive stresses. Within this context, the conditions for stable/unstable crack growth in the laminate can be directly established from Fig. 8, as has been nicely presented in recent work by Lugovy et al. [45]. Under a far-field applied stress intensity factor, K_{app}, given by the straight lines in Fig. 8, a crack with a crack length parameter P (i.e. below Q) will experience unstable propagation once the applied stress gets higher than σ_{p}. On the other hand, a crack with a crack length parameter R (i.e. above Q) will grow abruptly at a stress level σ_{r}, between points R and S, since the segment RS lies above the $K_{\mathrm{apt,c}}$. However, at point S, the
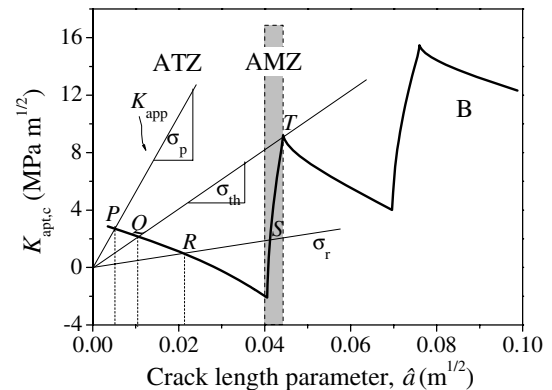

Fig. 8. Conditions for stable/unstable crack propagation in a layered structure type B with R-curve behaviour determined analytically using the weight function approach, as a function of a crack length parameter $\hat{a}$.

crack growth would become stable up to point T, i.e. any further crack advance will require an increase in the applied stress. Point T is a maximum value of $K_{apt,c}$ and it is located at the interface between the first AMZ and the second ATZ layer. As a consequence, it determines the threshold stress value, σ_{th}, above which the crack propagates unstably up to failure. For cracks with crack length parameters above T, crack extension takes place in a similar way as explained above, and the specimen failure is then dictated by the maximum value of $K_{apt,c}$ attained at the interface of the second AMZ and third ATZ layers.

Following the above ideas, small surface cracks located in the region of unstable growth will cause the catastrophic failure of the material when the fracture conditions for crack extension are satisfied, i.e. for an applied stress above the threshold stress. However, all cracks which are long enough to fall within the region of initial crack growth, will unstably propagate at the same stress level σ_{th}, i.e. the threshold strength. This prediction is sustained by the limit strength experimentally encountered for indented layered specimens, as shown in Fig. 7, where the failure stress of all specimens converged to the same value, regardless of the initial indentation flaw size.

This study has been extended to the other multilayered geometries, i.e. systems A and C, and all the results for $K_{apt,c}$ are shown in Fig. 9. It can be seen that $K_{apt,c}$ follows a similar trend for the three laminates investigated, showing a steep R-curve behaviour within the first AMZ compressive layer. Nonetheless, some differences may be discerned. For the cases of laminates A and B, apparent fracture toughness decreases from ∼3.2 MPa m$^{1/2}$ to negative values within the first ATZ layer until the crack reaches the first interface. This is explained by the relatively high residual tensile stresses present in the ATZ layers. Once the crack reaches the first interface, apparent toughness increases in the thin compressive layer region. The maximum $K_{apt,c}$ is observed for laminate A, due to the relatively thicker compressive AMZ layer, where the R-curve develops up to a value of 9.7 MPa m$^{1/2}$. It decreases again within the second ATZ tensile layer. The same trend may be dis-

cerned for systems B and C. However, the decrease in $K_{apt,c}$ is not so pronounced in system C since the tensile stresses in the corresponding ATZ layer are lower than in the other two systems. The negative values for $K_{apt,c}$ within the first ATZ layer of systems A and B would suggest spontaneous crack growth when the crack reached a certain crack length. As a matter of fact, this phenomenon has been experimentally observed and reported by the authors in a previous work [8]. In contrast, multilayered system C did not show negative values for $K_{apt,c}$, and consequently it did not reveal spontaneous crack growing in the experiments just discussed. Experimental data supporting the above ideas have been recently assessed by the authors for notched specimens, which showed no continuous growth of the initial crack [8]. Instead, the crack arising from the notch in the first ATZ layer starts to propagate, then gets arrested and finally continues its growth again. This crack arrest results in a "pop-in" event on the load–displacement curve, where an instantaneous drop in load may be observed.

In general, the estimated apparent fracture toughness values, $K_{apt,c}$, revealed an enhancement in the multilayer fracture behaviour with respect to the ATZ monolithic material taken as reference. However, no significant difference among the three layered structures was noted. In all cases, $K_{apt,c}$ was calculated at the first AMZ compressive layer, which acted as a barrier to any crack propagation. When the impinging crack entered this layer, bifurcation and/or deflection phenomena were discerned, yielding as a result a step-like fracture (Fig. 4). This is clear evidence of the complex mode of loading to which these materials may be subjected during fracture and thus the difficulty in the evaluation of the real fracture toughness of the multilayered structures. Hence, in order to assess the contribution of the rest of the layers to the crack resistance behaviour of each laminate system, COD-controlled tests were performed and the work of fracture evaluated for each multilayered architecture.

3.2.3. Work of fracture

The COD-controlled tests carried out on ATZ monoliths and laminates allowed one to evaluate the work of fracture required to break the samples. In the case of the ATZ monolith, the fracture initiated at the notch tip when reaching a certain opening displacement. As expected for a brittle material exhibiting a flat R-curve behaviour, failure associated with such first crack extension was already catastrophic (Fig. 10a). For the case of the laminates, crack growth originated also at the notch tip but at a stress value below the maximum one reached by the monolithic sample, as is clearly discerned from the first load drops in Fig. 10b–d. As has been discussed before, these differences are speculated to come from the tensile residual stresses inherent to the laminate at the notch site, which increase the effective stress intensity factor at that point. However, even though the crack started to grow at lower stress levels for the laminates, it did not produce catastrophic failure as in the case
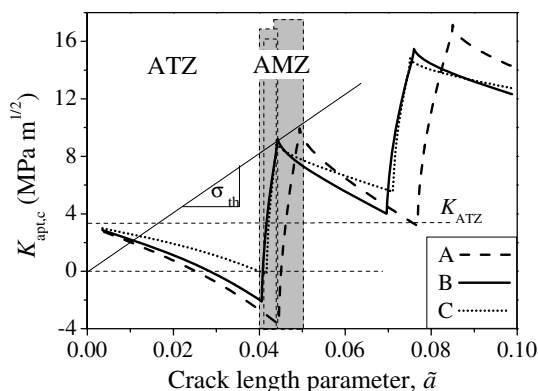

Fig. 9. Apparent fracture toughness, $K_{apt,c}$, calculated analytically using the weight function approach, considering the three different layered architectures, A, B and C.
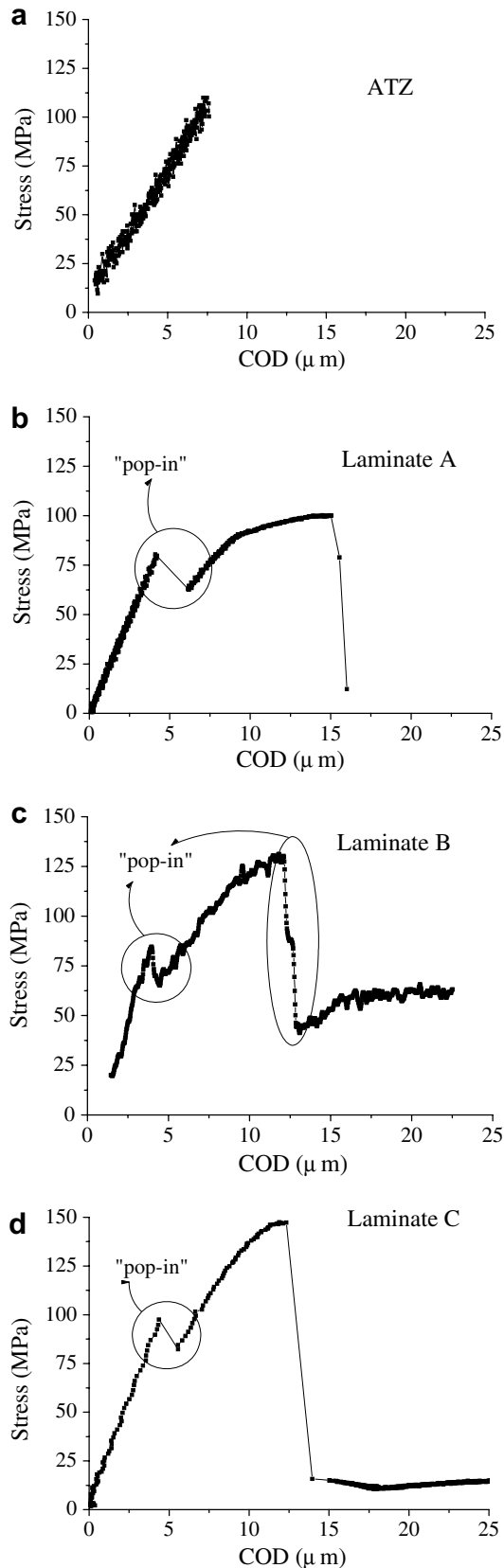
Fig. 10. Stress–COD response under COD control: (a) ATZ monoliths and (b–d) multilayered systems A, B and C, respectively. First "pop-in" event (only seen in the laminates) corresponds to the arrest, at the ATZ/AMZ interface, of the crack initiating from the notch tip.

of the monolith. Instead, cracks arrested at the first ATZ/AMZ interface, as in the case of the indentation strength tests presented above. As a direct consequence, in order to maintain the COD rate imposed during testing, a further applied load increase was required. Accordingly, there was a new rise in the stress–COD curve after the first drop in load, whose initial slope was directly dependent on how the effective stiffness of each multilayered configuration decreased with increasing crack extension. Additionally, as the crack propagated through the thin compressive layers, a further and continuous stress–COD slope reduction was discerned for all the laminates. Following the fractographic features evidenced in Fig. 4, such behaviour may be rationalized in terms of energy-absorbing mechanisms acting at the crack tip, such as crack deflection and/or bifurcation. Although these remarks were valid for all the multilayered systems, relative differences (although difficult to quantify) were also discerned among such analogous behaviour. For instance, in agreement with the more pronounced step-like fracture observed for laminates type A and B, with respect to the one exhibited by laminate C (Fig. 4), the stress–COD slope decrease following the first arrest in the former two is also more significant than for the latter. This is particularly true for laminate B where another crack arrest at the second ATZ/AMZ interface was also recorded. These subsequent steps increase the work of fracture of the material, i.e. the energy absorption capability associated with the layered architectural design.

Although it seems clear that the layer thickness ratio may influence the crack propagation through the multilayered material, it is difficult to account the contribution of each layer to the total work of fracture due to the complex failure mode of the composite. Assuming that all the work done was consumed in the growth of the crack and no significant elastic energy was stored in the specimen during testing, an assessment of the total work of fracture (γ_{WOF}) may be attempted through integration of the recorded load–COD curve per material volume unit for the ATZ monolith as well as for the three laminates [46]. The corresponding results are given in Table 4. As expected, γ_{WOF} values measured for the three laminates are significantly higher than the one determined for the ATZ monolith. Although the load–COD curve for the latter does not show a controlled crack growth, the γ_{WOF} value obtained for the ATZ monolith is in good agreement with those reported by other authors for pure alumina, indicating the utility of this approach [46]. For the laminates, two aspects may be highlighted: (i) the main contribution to the total work of fracture comes from the first AMZ layer, which acts as a barrier to crack propagation as discussed above, and (ii) the energy dissipated in systems B and C is about 40% and 30% higher, respectively, than in system A. The reasons for such behaviour are speculated to be different depending on the laminate. The increase in γ_{WOF} for layered systems type B is proposed to come from crack deflection induced at the ATZ/AMZ interface, and the corresponding bifurcation of the crack when entering the

thin compressive layers, where it propagates parallel to the layer plane, as depicted in Fig. 11. The higher value of γ_{WOF} for laminates type C is thought to result from the direct contribution of the first thin layer, whose residual compressive stress state is superior to that of laminates type A. In this case, energy-dissipating mechanisms such as crack bifurcation were much less pronounced, since the small thickness of the thin compressive layers is very close to the critical layer thickness below which such phenomenon is predicted not to occur [14]. Instead, crack propagation takes place through crack deflection mechanisms, and in some cases crack penetration, yielding as a result an almost straight fracture surface, as in the case of the ATZ monoliths.

Following the above ideas, it can be concluded that the work of fracture of the layered architectures investigated may be enhanced to levels up to six times that of the ATZ monolith, taken here as the reference material. From a practical viewpoint, the energy absorption capability of these structures will be higher than that of the constituent monoliths, leading to larger deformations before catastrophic failure under monotonic loading conditions. Looking at the crack extension mechanisms, it should be emphasized that the layer thickness ratio can be a significant parameter in the design of this type of layered structures. Particularly, the thickness of the internal compressive layers seems to play an important role since it should be the thinnest possible to provide high compressive stresses which act as a barrier against any possible on-growing surface defect, but at the same time thick enough to assure the development of toughening mechanisms such as crack bifurcation at fracture, which may increase considerably the energy absorption capability of the material. As a consequence, although layered architectures type C showed the best threshold strength values, the increase in the work of fracture associated with energy dissipating mechanisms, i.e. crack bifurcation, was found to be more significant for layered composites type B. Therefore, a multilayered design with nine alternating layers of the composition investigated and a layer thickness ratio between 5.7 (system B) and 9.5 (system C) may be proposed as an optimal choice for structural applications, when a combination of flaw tolerance and energy absorption capability is required.
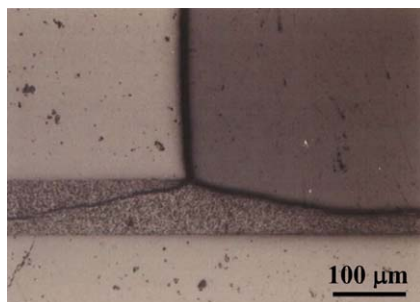

Fig. 11. Crack bifurcation at the thin compressive layers of a multilayer type B.

4. Conclusions

The Al$_2$O$_3$–ZrO$_2$ multilayers investigated exhibit an alternate tensile–compressive residual stress whose relative magnitudes are significantly dependent on the layer thickness ratio. As this parameter increases from 4.6 to 9.5, residual stresses decrease in the ATZ layers (including the surface one) from 116 to 60 MPa, whereas they increase from −680 to −720 MPa in the AMZ ones.

Although failure stress of the reference monolith is higher than that of the multilayered materials, the scatter in strength is much less in the latter. While the former is associated with different critical size defect, the latter is closely related to the toughening behaviour of laminated ceramics. This is explained by the observation of an arrest of the propagating initial natural flaws at the first compressive layer. Indentation-strength tests revealed the existence of a threshold strength inherent to the first compressive layers, regardless of the initial indentation-flaw sizes. This provides an increase in reliability for these multilayered structures in comparison to the reference monolith, being more significant in laminates with higher layer thickness ratio.

A crack growth resistance behaviour (R-curve), effectively evaluated through a weight function approach, was observed in the three laminates of study compared to the brittle fracture of the reference monolith. Although the apparent fracture toughness decreases within the tensile layers, a significant increase when the crack enters the thin compressive layers is observed. Toughness values of the layered architectures were up to three times that of the reference monolith, and the work of fracture enhanced to levels up to six times, being more significant for systems with higher compressive stresses (systems B and C).

Fractographic observations indicate crack bifurcation, associated with the high compressive stress state and layer thickness, as the mechanism responsible for such increase in fracture energy. Nonetheless, the step-like fracture observed in the laminates is not so pronounced in the system with higher layer thickness ratio (system C). Hence, it is suggested that not only the absolute value of the thickness ratio conditions the fracture behaviour of multilayered structures but also the thickness of the internal thin compressive layers. As a consequence, although layered architectures type C showed the best threshold strength values, the increase in the work of fracture associated with crack bifurcation mechanisms was found to be more significant for layered composites with thickness ratios between systems B and C. Hence, a multilayered design of nine alternating layers of the composition investigated with a layer thickness ratio between 9.5 and 5.7 is proposed as an optimal choice for structural applications, when a good combination of flaw tolerance and energy absorption capability is attempted.

Acknowledgements

References

[1] Virkar AV, Huang JL, Cutler RA. J Am Ceram Soc 1987;70:164.
[2] Marshall DB, Ratto JJ, Lange FF. J Am Ceram Soc 1991;74:2979.
[3] Katsuki H, Hirata Y. J Ceram Soc Jpn 1990;98:1114.
[4] Hansen JJ, Cutler RA, Shetty DK, Virkar AV. J Am Ceram Soc 1988;71:501.
[5] Lakshminarayanan R, Shetty DK, Cutler RA. J Am Ceram Soc 1996;79:79.
[6] Rao MP, Sánchez-Herencia AJ, Beltz GE, McMeeking RM, Lange FF. Science 1999;286:102.
[7] Sglavo VM, Paternoster M, Bertoldi M. J Am Ceram Soc 2005;88:2826.
[8] Bermejo R, Torres Y, Sánchez-Herencia AJ, Pascual J, Anglada M, Llanes L. J Eur Ceram Soc, (2006), doi:10.1016/j.jeurceramsoc.2006.05.037.
[9] Sánchez-Herencia AJ, Moya JS, Tomsia AP. Scripta Mater 1997;38:1.
[10] Krishnamurthy R, Sheldon BW. Acta Mater 2004;52:1807.
[11] He MY, Hutchinson JW. Int J Solids Struct 1989;25:1053.
[12] Phillips AJ, Clegg WJ, Clyne TW. Acta Metall Mater 1993;41:805.
[13] Kuo DH, Kriven WM. Mater Sci Eng 1998;241:241.
[14] Oechsner M, Hillman C, Lange FF. J Am Ceram Soc 1996;79:1834.
[15] Sánchez-Herencia AJ, James L, Lange FF. J Eur Ceram Soc 2000;20:1297.
[16] Clegg WJ, Kendall K, Alford NM, Button TW, Birchall JD. Nature 1990;347:455.
[17] Sánchez-Herencia EG, Pascual C, He J, Lange FF. J Am Ceram Soc 1999;82:1512.
[18] Pontin MG, Rao MP, Sánchez-Herencia AJ, Lange FF. J Am Ceram Soc 2002;85:3041.
[19] Bermejo R, Llanes L, Baudín C, Moreno R, Sánchez-Herencia AJ. Comp Sci Tech, submitted for publication.
[20] Requena J, Moreno R, Moya JS. J Am Ceram Soc 1989;72:1511.
[21] Oel HJ, Fréchette VD. J Am Ceram Soc 1967;50:542.
[22] Chartier T, Merle D, Besson JL. J Eur Ceram Soc 1995;15:101.
[23] Anstis GR, Chantikul P, Lawn BR, Marshall DB. J Am Ceram Soc 1981;64:533.
[24] Marshall DB, Lawn BR. J Mater Sci 1979;14:2001.
[25] Bermejo R, Torres Y, Sánchez-Herencia AJ, Baudín C, Anglada M, Llanes L. Fatigue Fract Eng Mater Struct 2006;29:71.
[26] Bermejo R, Llanes L, Anglada M, Supancic P, Lube T. Key Eng Mater 2005;290:191.
[27] Sergo V, Lipkin DM, De Portu G, Clarke DR. J Am Ceram Soc 1997;80:1633.
[28] Timoshenko SP, Goodier JN. Theory of elasticity. New York (NY): McGraw-Hill; 1987. p. 104.
[29] Zimmermann A, Hoffman M, Flinn BD, Bordia RK, Chuang T-J, Fuller Jr ER, Rödel J. J Am Ceram Soc 1998;81:2449.
[30] Casellas D, Alcalá J, Llanes L, Anglada M. J Mater Sci 2001;36:3011.
[31] Baratta FI. J Am Ceram Soc 1981;64:C-3.
[32] Fett T. Int J Fract 1994;67:R–41.
[33] Kirchner HP, Gruver RM, Sotter WA. Mater Sci Eng 1976;22:147.
[34] Baratta FI. J Am Ceram Soc 1978;61:90.
[35] Kirchner HP, Gruver RM. J Mater Sci 1979;14:2110.
[36] Heinrich J, Munz D. Am Ceram Soc Bull 1980;59:1221.
[37] Newman J, Raju I. Eng Fract Mech 1981;15:185.
[38] Ho S, Hillman CD, Lange FF, Suo Z. J Am Ceram Soc 1995;78:2353.
[39] Pontin MG, Lange FF. J Am Ceram Soc 2005;88:376.
[40] Marshall DB, Lawn BR, Chantikul P. J Mater Sci 1979;14:2225.
[41] Fett T, Munz D. Stress intensity factor and weight functions. Southampton: Computational Mechanics Publications; 1997. p. 408.
[42] Strawley JE. Int J Fract 1976;12:475.
[43] Rao MP, Rödel J, Lange FF. J Am Ceram Soc 2001;84:2722.
[44] Moon R, Hoffman M, Bowman JH, Trumble K, Rödel J. J Am Ceram Soc 2002;85:1505.
[45] Lugovy M, Slyunyayev V, Orlovskaya N, Blugan G, Kübler J, Lewis M. Acta Mater 2005;53:289.
[46] Tattersall HG, Tappin G. J Mater Sci 1966;1:296.